Published in final edited form as:
J Phys Chem B. 2011 June 23; 115(24): 7996–8003. doi:10.1021/jp202024x.

Optically-Enhanced, Near-IR, Silver Cluster Emission Altered by Single Base Changes in the DNA Template

Jeffrey T. Petty[1], **Chaoyang Fan**[2], **Sandra P. Story**[1], **Bidisha Sengupta**[1], **Matthew Sartin**[2], **Jung-Cheng Hsiang**[2], **Joseph W. Perry**[2], and **Robert M. Dickson**[2,3]

Jeffrey T. Petty: jeff.petty@furman.edu; Robert M. Dickson: dickson@chemistry.gatech.edu

[1]Department of Chemistry, Furman University, Greenville, SC 29613

[2]School of Chemistry and Biochemistry, Georgia Institute of Technology, Atlanta, GA 30332-0400

[3]Petit Institute for Bioengineering and Bioscience, Georgia Institute of Technology, Atlanta, GA 30332-0400

Abstract

Few-atom silver clusters harbored by DNA are promising fluorophores due to their high molecular brightness along with their long- and short-term photostability. Furthermore, their emission rate can be enhanced when co-illuminated with low-energy light that optically depopulates the fluorescence-limiting dark state. The photophysical basis for this effect is evaluated for two near infrared-emitting clusters. Clusters emitting at ~800 nm form with $C_3AC_3AC_3TC_3A$ and $C_3AC_3AC_3GC_3A$ and both exhibit a trap state with λ_{max} ~ 840 nm and an absorption cross section of 5–6 × 10^{-16} cm^2/molec that can be optically depopulated. Transient absorption spectra, complemented by fluorescence correlation spectroscopy studies, show that the dark state has an inherent lifetime of 3–4 μs and that absorption from this state is accompanied by photoinduced crossover back to the emissive manifold of states with an action cross section of ~2 × 10^{-18} cm^2/molec. Relative to $C_3AC_3AC_3TC_3A$, $C_3AC_3AC_3GC_3A$ produces a longer-lived trap state and permits more facile passage back to the emissive manifold. With the $C_3AC_3AC_3AC_3G$ template, a spectrally distinct cluster forms having emission at ~900 nm and its trap state has a ~four-fold shorter lifetime. These studies of optically-gated fluorescence bolster the critical role of the nucleobases on both the formation and excited state dynamics of these highly emissive metallic clusters.

Keywords

Silver Cluster; Optically-Gated Fluorescence; DNA Templates

Introduction

Fluorescence imaging opens a mechanistic window on biological processes through its ability to temporally and spatially resolve biochemical events with molecular specificity.[1,2] The development of fluorescent biological labels has yielded access to a broad spectrum of biological events, combining high sensitivity with minimal perturbation. High fluorophore brightness is attainable using lasers to drive electronic transitions, often producing bright integrated and spectrally resolved emission.[3] However, emission rate is too-often limited by photoinduced excursions from the fluorescent manifold of states, as evidenced by plateaus in emission intensity and corresponding fluorescence intensity fluctuations.[4–7] This dark-state

Correspondence to: Jeffrey T. Petty, jeff.petty@furman.edu; Robert M. Dickson, dickson@chemistry.gatech.edu.

shelving coupled with relatively long lifetimes in these nonemissive states severely restrict obtainable molecular emission rates. Furthermore, enhanced photobleaching from excited electronic states limits observation times. These detrimental effects can be partially ameliorated using oxidizing and reducing agents to interrupt electron transfer that may sometimes be associated with fluorescence quenching.[8–10] Such additives are designed to suppress triplet populations while also regenerating the chromophore in the singlet electronic state, but their introduction may also perturb the system under study and possibly quench emission. Thus, each chromophore and imaging experiment must be evaluated individually to balance these effects.

Circumventing chemical approaches, populations in dark electronic states can also be optically regulated.[11–15] One approach uses sequential excitation to induce crossover from transiently stable dark states back to the emissive manifold of states via coupling with higher lying electronic levels. Rapid passage back to the emissive manifold thus increases emission intensity by increasing steady-state population of fluorescence-generating molecules. This enhancement depends on the natural lifetime of the dark state and rates of forward and reverse dark state crossings. The power of optically modulating dark state populations is realized when a primary laser produces fluorescence and a secondary laser at a different wavelength depopulates the dark state.[16] For fluorescence imaging, this approach avoids a great deal of the fluorescence background that is inherent in biological systems. Further augmenting the gains from high energy photoswitches,[16] even greater sensitivity enhancements are realized by wavelengths longer than fluorescence for optical depopulation of transient dark states.[13] As the low energy secondary laser does not increase the fluorescent background, target fluorescence is externally modulated and distinguished from the total background.

DNA-templated silver clusters are a recently developed class of fluorophore that are particularly responsive to optical modulation of their emission. Like their Ag^+ precursor, reduced silver clusters are stabilized both locally and globally by the electron-rich nucleobases.[17–19] Within oligonucleotide templates, sequence variations yield specific clusters with distinct emission spanning the blue-green to near-infrared spectral region.[20–22] Chemical reduction of oligonucleotide-complexed Ag^+ typically produces a range of absorbing species, clouding cluster size determinations for the emissive species, unless purification and elemental analysis can be performed.[22,23] These, coupled with size, pH and spectroscopic studies all indicate Ag cluster complexation with the bases of intact ssDNA.[20,24]

As bright near infrared emitters are both important and scarce, we have recently focused on silver clusters with near-infrared electronic transitions.[22] In parallel with a favorable molecular brightness (product of extinction coefficient and fluorescence quantum yield) of 60,000 M^{-1} cm^{-1}, especially when compared with spectrally similar emitters,[25] this cluster has a short ~μsec dark state lifetime that facilitates both high sustained emission rates relative to more standard dyes such as Cy7 and fluorescence enhancement using dual excitation by short and long wavelength lasers. The present studies investigate the role of subtle base modifications on bright and (optically modulatable) dark state cluster photophysics in a newly identified family of related near-infrared emitting silver clusters. This family is based on the previously identified sequence $C_3AC_3AC_3XC_3Y$,[22] but with varied bases at the X and Y positions to significantly alter bright and dark state photophysics. Spectroscopic investigations of dark state absorption are particularly relevant to the fluorescence enhancement, and, like the ground state absorption, are shown to significantly alter dark state kinetics and energetics. These variations in the primary sequence further establish how the ssDNA template dictates the excited state dynamics of emissive silver clusters. [13,14]

Experimental Methods

Silver nitrate (Aldrich, 99.9999%) and sodium borohydride (Aldrich, 99%) were used as received. Oligonucleotides (Integrated DNA Technologies and Operon) were purified by desalting by the manufacturer and dissolved in sterilized, deionized water (Barnstead Nanopure ultrapure water system). DNA concentrations were determined by absorbance using molar absorptivities based on the nearest-neighbor approximation.[26] Silver nanoclusters were synthesized by mixing an oligonucleotide and $AgNO_3$ solution for 15 sec in 10 mM citrate buffer at pH = 7, then followed by addition of an aqueous $NaBH_4$ solution. The resulting solution was vigorously shaken for 1 min. Samples were analyzed after reaction for 8 hours. The oligonucleotide concentrations were either 15 or 300 μM with relative molar amounts of 8 Ag^+ and 4 BH_4^-. To emphasize the position in the primary sequence that has been modified, the relevant bases are underlined.

Visible absorption spectra were acquired using a Varian Cary 50 Bio UV-Visible and a Shimadzu UV-2401 PC spectrophotometer. Fluorescence spectra were acquired on Jobin Yvon Horiba Fluoromax-3 and Photon Technology International QuantaMaster spectrofluorimeters. Correspondence between the excitation and absorption bands in the near infrared allowed the fluorescence quantum yield to be measured using Cy7 ($\Phi_f = 0.13$) and Indocyanine Green as ($\Phi_f = 0.04$) reference chromophores.[27,28] Reversed-phase ion-pair chromatography was performed with a Shimadzu Prominence HPLC system using a semi-prep Gemini C18 column, which is 50 mm long and 10 mm internal diameter and has particles with an average size of 5 μm and a pore size of 110 Å (Phenomenex). The mobile phase was 35 mM triethylamine acetate at pH = 7 and methanol, with a linear gradient of 10%–30% methanol over 8 min followed by a 3 min hold at 10% methanol at a flow rate of 5 mL/min. Separations were conducted at 25 °C. Absorption and fluorescence measurements of the separated species were made using the SPD-M20A and RF-10XL detectors, respectively. Using a FRC-10A fraction collector, the solutions containing the isolated cluster-DNA conjugate were dehydrated and dissolved in water containing 0.8 M nitric acid. After HPLC purification, the quantities of silver and phosphorous were determined by inductively coupled plasma-atomic emission spectroscopy (Optima 7300 DV, Perkin Elmer). To account for different detection efficiencies, control samples comprised of known relative amounts of Ag^+ and encapsulating 16-based oligonucleotide were used. To determine the oligonucleotide concentration, the stoichiometry of 15 phosphorous atoms per oligonucleotide was used, which accounts for the absent terminal 3′-phosphate.

Fluorescence correlation spectroscopy studies were conducted using diode laser excitation at 690, 840, and 905 nm with current and temperature control (LTC100, Thorlabs). A 63× 1.2 NA water immersion microscope objective (Zeiss) in a laser epi-illuminated geometry excited the sample and collected the fluorescence. A long-pass dichroic (Semrock) was used to reflect the laser into the back of the objective and transmit the emission, which was spectrally filtered before coupling into a 50-μm diameter fiber located at the image plane of the microscope. The fiber was coupled to actively-quenched single-photon counting avalanche photodiode detectors (SPCMAQR14, Perkin Elmer) using a Hanbury Brown-Twiss setup.[29] The resulting TTL signal outputs were cross correlated (Correlator.com) to give an autocorrelation free of afterpulsing artifacts, thereby improving time resolution. To determine the cluster concentrations, dilute solutions of Cy7 and Indocyanine Green were used as reference fluorophores to determine the probe volume dimensions using a 3-D Gaussian model. [22,30]

As described in earlier studies, time resolved nanosecond absorption spectra were conducted as pump-probe experiments.[14] The pump laser was operated at 740 nm with an energy of 700 μJ. The fluorescence lifetime was measured using a mode-locked Ti- Sapphire laser

(Coherent Mira) with a pulse-picker for adjusting the repetition rate (ConOptics). TTL signals were processed with a photon counting module (SPC-630, Becker Hickl or PicoHarp E, PicoQuant). Fluorescence decays accounted for convolution of the fluorescence decay with the measured instrument response function.

Results

$C_3AC_3AC_3TC_3A$

The emission at 810 nm from the Ag_{10}-conjugate formed in $C_3AC_3AC_3TC_3A$ is increased when 905 nm irradiation accompanies the primary excitation at 690 nm.[22] Time-resolved transient absorption spectroscopy indicates that this enhancement arises from long-wavelength depopulation of a low yield, long-lived, and non-emissive excited state that is weakly coupled to the emissive manifold of states (Fig. 1 and 2). In the μs time regime, a ground-state bleach with a wavelength minimum that coincides with the λ_{max} in the absorption spectrum is accompanied by an excited-state absorption with a maximum absorbance change at 833 nm. Direct coupling of this excited dark state with the ground state is indicated by the single exponential relaxation with a time constant of ~3 μs and an isosbestic point at 801 nm between the two bands. Given this two-state conversion, extinction coefficients of the excited and ground states are equal at this common intersection of their spectra.[31] Based on the previously measured ground state absorption cross section of 7 (± 2) × 10^{-16} cm^2 $molec^{-1}$ at 750 nm[22] and accounting for the profiles of the ground state and excited state absorption bands, the excited state absorption cross-section at λ_{max} = 833 nm is 6 (± 2) × 10^{-16} cm^2 $molec^{-1}$.

A fuller picture of the excited state dynamics and dual excitation-based photobrightening is obtained by two-color fluorescence correlation spectroscopy (Fig. 3). Fluorescence fluctuations in the 0.1 – 10 μs time range occur much faster than translational diffusion through the optically-defined probe volume (~400 μs). Thus, autocorrelation analysis of the time-dependent fluorescence changes is resolvable into diffusive ($g_D(\tau)$) and excited state ($g_{ES}(\tau)$) contributions:[12]

$$G(\tau)=1+\frac{1}{N}g_D(\tau)g_{ES}(\tau)$$

where $g_{ES}(\tau)$ is:

$$g_{ES}(\tau)=1+\frac{F}{1-F}e^{-\tau/\tau_{ES}}$$

in which F is the fractional occupancy of the dark state and τ_{ES} is the net correlation time for dark state shelving. In conjunction with 690 nm excitation within the emissive manifold of states, secondary excitation at 905 nm selectively excites the dark state. Based on the time-resolved absorption spectra, absorption at 905 nm is expected to produce significant excitation of the dark state population with minimal ground state excitation (Fig. 2). This selective photoexcitation is evident by decomposing the observed correlation times (τ_{ES}) into entrance times to (τ_{on}) and exit times from (τ_{off}) the dark state as a function of secondary laser irradiance (Table 1).[32] The τ_{on} values are not greatly perturbed by the secondary laser, consistent with its energy being off-resonance relative to ground state excitation. In contrast, τ_{off} values decrease with irradiance at the longer wavelength, supporting selective dark state depopulation. Mechanistic perspective is provided using the following reaction scheme:[12]

$$\text{Emissive Manifold} \underset{k_{DS}}{\overset{k_{SD}}{\rightleftharpoons}} \text{Dark Manifold}$$

In this model, the emissive state is strongly coupled with the ground state, and the dark state is weakly coupled to the emissive manifold as described by the relatively small rate constants k_{SD} and k_{DS} for entering into and exiting from the dark state, respectively (Fig. 3). Assuming identical diffusion coefficients associated with these two states, a kinetic analysis relates the net correlation time (τ_{ES}) and the steady-state fractional occupancy (F) to the rate constants:[12]

$$k_{DS} = \frac{1-F}{\tau_{ES}}$$
$$k_{DS} = k_{DS}^{o} + \sigma\gamma I$$

where k_{DS}^{o} is the inherent dark state decay rate constant due solely to nonradiative relaxation, σ(cm^2/molec) is the action cross section for reverse intersystem crossing back to the singlet manifold, γ (photon/J) is $(h\nu)^{-1}$, and I is the secondary laser irradiance (W/cm^2). Based on how the observed rate constant varies with a ten-fold variation in the irradiance of the secondary beam, an inherent decay rate constant of 3.0 (±0.1) × 10^5 s^{-1} with a corresponding time constant of 3.3 μs is obtained (Fig. 3). The slope provides the action cross section for reverse crossing, and the value of 0.015 (± 0.002) × 10^{-16} cm^2/molec is comparable to values previously measured for organic chromophores.[12]

$C_3AC_3AC_3GC_3A$

Within the general sequence $C_3AC_3AC_3XC_3A$, the three remaining oligonucleotides with X = G, C, and A were investigated. Relative to the thymine derivative discussed above, these modifications produce clusters with similar absorption and fluorescence spectra, thus indicating that essentially the same silver cluster forms with all these templates. Because the oligonucleotides containing thymine and guanine are distinguished by their chemical stability, the subsequent discussion focuses on the photochemical and chemical characteristics of the cluster that forms with $C_3AC_3AC_3\underline{G}C_3A$ that emits at 770 nm (Fig. 3). As with $C_3AC_3AC_3\underline{T}C_3A$,[22] a mixture of species forms with $C_3AC_3AC_3\underline{G}C_3A$, but these can be separated by reversed-phase HPLC (Fig. 4). Of the three primary species, the near-infrared emitting species is identified by its fluorescence response and associated absorption feature at 720 nm. The absorption spectrum shows that the ubiquitous absorbance at ~400 nm in as-synthesized samples is removed through purification, with only the near IR cluster and UV DNA absorptions remaining. Using atomic emission spectroscopy to quantify the amounts of phosphorous and silver, the known phosphate content of the oligonucleotide was used to determine a relative stoichiometry of 10.0 ± 1.7 Ag:$C_3AC_3AC_3\underline{G}C_3A$, which is similar to the value of 9.6 ± 0.8 Ag previously reported for similarly emitting clusters in $C_3AC_3AC_3\underline{T}C_3A$ [22]. Relative to $C_3AC_3AC_3\underline{T}C_3A$, the guanine containing oligonucleotide encapsulates a cluster with a similar fluorescence quantum yield of 30 ± 5% and a comparable lifetime of 2.2 ns. Despite these stoichiometry and photophysical similarities, the cluster environment is influenced by nucleobase substitution, as illustrated by the absorption cross section. Identified by its fluorescence signature, the cluster concentration was quantified using the amplitude of the diffusive component of the fluorescence correlation function, and the optically defined probe volume was calibrated using solutions of Cy7 concentration standards.[33] Cluster occupancy varied linearly with dilution, thus enabling extrapolation to the concentrations used for absorbance. The resulting absorption

cross section of 3.2 (± 0.4) × 10^{-16} cm^2 $molec^{-1}$ at 720 nm is only about 50% of that measured for the $C_3AC_3AC_3\underline{T}C_3A$-templated cluster, but the resulting molecular brightness ($\Sigma \times \Phi_{fl}$) of 24,000 M^{-1} cm^{-1} again compares favorably to chromophores in this spectral region.[25]

Further effects of the cluster environment are evident in the excited state dynamics. Time-resolved absorption and fluorescence correlation spectroscopy studies show that the cluster associated with $C_3AC_3AC_3\underline{T}C_3A$ and $C_3AC_3AC_3\underline{G}C_3A$ exhibit similar dark state characteristics, but branching out of this state is affected by base identity at the 12th nucleotide. Spectral decomposition of the time-resolved absorption data identifies the ground state bleach and an excited state absorption (Fig. 2). The λ_{max} = 841 nm for the dark state absorption feature is similar to that observed for clusters within $C_3AC_3AC_3\underline{T}C_3A$. Two-state relaxation is again supported by monoexponential decay from the excited state and by an isosbestic point having ΔOD = 0 at 778 nm between the bleach and absorption bands, and the latter observation yields an excited state absorption cross section of 4.8 (±0.5) × 10^{-16} cm^2/molec at 841 nm. Escape efficiency from the dark state depends on the DNA sequence, as shown by fluorescence correlation spectroscopy (Fig. 3). Using the two-laser excitation scheme with varying excitation rates at 905 nm in conjunction with fixed intensity primary excitation at 690 nm for the $C_3AC_3AC_3\underline{G}C_3A$encapsulated silver cluster, we find that τ_{on} values are not altered by a ten-fold increase in the irradiance at 905 nm while the τ_{off} values decrease (Table 1). By analyzing the irradiance dependence of observed decay rate constants, an inherent relaxation rate constant of 2.4 (± 0.2) × 10^5 s^{-1} with an associated time constant of 4.2 μs is measured, and this rate is ~20% slower relative to that measured for clusters in $C_3AC_3AC_3\underline{T}C_3A$. The resulting action cross section for reverse intersystem crossing is 0.022 (± 0.002) × 10^{-16} cm^2 $molec^{-1}$, which is ~50% higher than that formed in $C_3AC_3AC_3\underline{T}C_3A$. This cluster species is also distinguished by its larger relative enhancement derived from τ_{off} and τ_{on}. Based on a three-level system with both natural and photoinduced loss from the dark state, the enhancement achieved using dual vs. single laser excitation in the limit of low excitation rate is:

$$\text{Relative Enhancement} = \frac{I_F^{\text{Dual Laser}} - I_F^{\text{Single Laser}}}{I_F^{\text{Single Laser}}} = \frac{\tau_{off}^0 - \tau_{off}}{\tau_{on} + \tau_{off}}$$

where $I_F^{\text{Dual Laser}}$ and $I_F^{\text{Single Laser}}$ are the fluorescence intensities using dual and single laser excitation, respectively and $\tau_{off}^0 = 1/k_{DS}^0$ represents the time for strictly natural decay from the dark state. The comparable on times but longer off times of clusters in $C_3AC_3AC_3\underline{G}C_3A$ relative to those in $C_3AC_3AC_3\underline{T}C_3A$ suggests a cluster environment that is more amenable to fluorescence brightening by the secondary laser (Fig. 3 and Table 1).

$C_3AC_3AC_3AC_3G$

A primary feature of DNA-templated silver clusters is the profound effect of base sequence on cluster type.[20] Further consideration of sequence effects shows that the ~800 nm emitter also forms with X = A, T, and C in $C_3AC_3AC_3AC_3X$, yet a distinct species emitting at 900 nm forms with X = G (Fig. 3). With this template, four major species are chromatographically separated, and the new cluster is identified by its spectral signatures (Fig. 4). Atomic emission studies following chromatographic isolation gives a stoichiometry of 9.1 ± 0.5 Ag:$C_3AC_3AC_3AC_3\underline{G}$. Thus, the 800-nm emitters are both consistent with 9 or 10 Ag atom clusters, while the 900-nm emitter is only consistent with a 9-Ag atom species. Beyond the spectral distinctions, the cluster that forms with $C_3AC_3AC_3AC_3\underline{G}$ is further distinguished by its emissive and dark state photophysics. Relative to the ~800 nm emitter

that forms with $C_3AC_3AC_3\underline{G}C_3A$, the ~900 nm emitter has a five-fold lower fluorescence quantum yield (6 ± 2 %) and a five-fold higher absorption cross section (16.8 (± 1.1) × 10^{-16} cm^2 $molec^{-1}$ at λ_{max} = 840 nm). Together, the resulting molecular brightness of 26,000 M^{-1} cm^{-1} and short fluorescence lifetime of 1.4 ns again make this a promising chromophore to complement the limited choices of chromophores in this spectral region.[25] Fluorescence correlation studies show weak coupling to a dark state, but the rate of relaxation is faster for the ~900 nm emitter relative to those of the ~800 nm emitters (Fig. 3 and Tables 1 and 2). Irradiance measurements at 840 nm show an inherent decay rate constant of 9.4 (± 1.7) × 10^5 s^{-1} with a corresponding time constant of 1.1 μs. Evidence of an optical contribution to the excited dark state dynamics, however, is provided by the τ_{on} and τ_{off} times (Table 2). Coupled with the greater primary laser-induced excitation rate, the probability of entering the dark state increases at higher irradiances. In tandem, the exit rates increase with primary laser irradiance, suggesting that primary excitation laser also accelerates dark state depletion. Efforts to spectroscopically identify this state were hampered by the ground state and dark state spectral overlap, as indicated by the τ_{on} and τ_{off} values for single laser excitation (Table 2).

Discussion

A key observation from our studies is that dark electronic states in near infrared emitting silver clusters can be optically manipulated to enhance fluorescence through increasing steady-state population within the fluorescent manifold of states.[11–13] Optically induced excited state depopulation allows these relaxation pathways to be deciphered, while simultaneously demonstrating that emission is enhanced by repopulating the emissive manifold. Spurred by the desire to enhance label visibility for fluorescence imaging, a broad study of chromophores revealed that the degree of reverse intersystem crossing and hence fluorescence enhancement is specific to the dye, to its wavelength for excitation out of the triplet state, and to its environment.[12] With most of these systems, effective cross sections for reverse intersystem crossing of 10^{-19} - 10^{-18} cm^2/molec are derived from kinetic modeling.[12,34]

Dark electronic states in DNA-conjugated silver clusters can also be optically addressed.[13,14,22] For clusters that emit at ~700 nm, a charge-transfer state is supported by a large change in the dipole moment, and cytosine anion-suggestive transient absorption spectra.[14] Our time-resolved absorption spectra demonstrate that near infrared emitting silver clusters conjugated with $C_3AC_3AC_3\underline{T}C_3A$ and $C_3AC_3AC_3\underline{G}C_3A$ exhibit similar dark electronic state characteristics with λ_{max} ~ 840 nm, and with absorption cross sections of 5–6 × 10^{-16} cm^2/molecule. Photophysically distinct from the shorter wavelength emitters studied previously, the dark states of the longer-wavelength emitting, 9 – 10 atom clusters relax with time constants of 3 – 4 μs, and can be optically promoted using a second, lower energy laser. The net emission rate is enhanced because the steady state population within the fluorescent state manifold is increased due to optical depopulation of the transient dark state, having an action cross section of ~10^{-18} cm^2/molec at 905 nm. This value is comparable to reverse intersystem crossing cross sections exhibited by organic fluorophores, thereby supporting efficient enhancement of emission via optical methods.[12] Insight into the nature of the dark electronic state is provided by comparison with previously studied red emitters which have a broad transient absorption band centered at ~650 nm ascribed to electron transfer from the cluster to the cytosine nucleobase.[14] The ~800 nm emitters are distinguished by their relatively narrow transient absorption feature at ~840 nm that may be enveloped by the broader transition observed for the ~700 nm emitters. For both emitters, dark state excitation energies could feasibly promote oxidation of these small clusters.[14,35]

In addition to demonstrating long-wavelength optically enhanced near IR fluorescence, another key observation is the impact of the nucleobase environment. Comparing the clusters that form in $C_3AC_3AC_3TC_3A$ and $C_3AC_3AC_3GC_3A$, the guanine derivative has a longer transient lifetime within and a higher action cross section for reverse crossing out of the dark state, thereby leading to its greater degree of fluorescence enhancement. Furthermore, primary sequence effects on the types of clusters that form also extend to the near infrared, as demonstrated by the formation of a new near infrared emitter with emission at 900 nm using $C_3AC_3AC_3AC_3G$. Not only is the energy spacing in the emissive states influenced, but the excited state dynamics are distinguished by the short lifetime. These observations suggest that both stabilization of particular clusters and their excited state properties are dictated by the nucleobase interactions that direct cluster formation.

Conclusion

The primary conclusion from our steady state, transient absorption, and fluorescence correlation spectroscopy studies is that nucleobase sequence dictates the types of templated clusters and their excited state dynamics. Within the general sequence $C_3AC_3AC_3XC_3Y$, the DNA-templated clusters exhibit emissions at ~800 and ~900 nm with (X, Y) = (T/G, A) and (X, Y) = (A, G), respectively. The excited electronic states of these emissive metallic clusters couple to trap states, and lifetimes in these states also depend on the base sequence of the encapsulating oligonucleotide. Complementing this ability to optically gate emission using long wavelength excitation out of a transiently populated dark state, these fluorophores also display relatively high molecular brightness ($>10^4\ M^{-1}cm^{-1}$) in the biologically important near infrared spectral range. These characteristics portend the promise of DNA-templated silver clusters as fluorescent labels.

Acknowledgments

We thank the National Science Foundation (CBET-0853692) for support of this work. JTP is grateful to the National Institutes of Health (R15GM071370) for primary support during the initial stages of this work. In addition, JTP thanks the National Science Foundation (CHE-0718588), Henry Dreyfus Teacher-Scholar Awards Program, and the National Institutes of Health (P20 RR-016461 from the National Center for Research Resource). RMD acknowledges NIH R01-GM086195. JTP received partial sabbatical support through matching commitments to an NSF RII Cooperative Agreement, EPS- 0903795. JWP gratefully acknowledges support from the Army Research Office Multidisciplinary University Research Initiative (Grant No. 50372-CH-MUR). We thank Dr. Joel Hales for discussions and assistance with transient absorption measurements.

References

1. Tsien RY. Nat Rev Mol Cell Biol. 2003; 4:SS16. [PubMed: 14587522]
2. Aalberts DP, Parman JM, Goddard NL. Biophys J. 2003; 84:3212. [PubMed: 12719250]
3. Lord SJ, Lee H-lD, Moerner WE. Anal Chem. 2010; 82:2192. [PubMed: 20163145]
4. Rasnik I, McKinney SA, Ha T. Nat Methods. 2006; 3:891. [PubMed: 17013382]
5. Basche T, Kummer S, Brauchle C. Nature. 1995; 373:132.
6. Xie XS, Trautman JK. Annu Rev Phys Chem. 1998; 49:441. [PubMed: 15012434]
7. Widengren J, Mets U, Rigler R. J Phys Chem. 1995; 99:13368.
8. Vogelsang J, Kasper R, Steinhauer C, Person B, Heilemann M, Sauer M, Tinnefeld P. Angew Chem Int Ed. 2008; 47:5465.
9. Widengren J, Chmyrov A, Eggeling C, Löfdahl P-Å, Seidel CAM. J Phys Chem A. 2006; 111:429. [PubMed: 17228891]
10. Cordes T, Vogelsang J, Tinnefeld P. J Am Chem Soc. 2009; 131:5018. [PubMed: 19301868]
11. Redmond RW, Kochevar IE, Krieg M, Smith G, McGimpsey WG. J Phys Chem A. 1997; 101:2773.

12. Ringemann C, Schönle A, Giske A, von Middendorff C, Hell SW, Eggeling C. ChemPhysChem. 2008; 9:612. [PubMed: 18324718]
13. Richards CI, Hsiang JC, Senapati D, Patel S, Yu J, Vosch T, Dickson RM. J Am Chem Soc. 2009; 131:4619. [PubMed: 19284790]
14. Patel SA, Cozzuol M, Hales JM, Richards CI, Sartin M, Hsiang JC, Vosch T, Perry JW, Dickson RM. J Phys Chem C. 2009; 113:20264.
15. Heilemann M, Dedecker P, Hofkens J, Sauer M. Laser Photon Rev. 2009; 3:180.
16. Marriott G, Mao S, Sakata T, Ran J, Jackson DK, Petchprayoon C, Gomez TJ, Warp E, Tulyathan O, Aaron HL, Isacoff EY, Yan Y. Proc Natl Acad Sci U S A. 2008; 105:17789. [PubMed: 19004775]
17. Ritchie CM, Johnsen KR, Kiser JR, Antoku Y, Dickson RM, Petty JT. J Phys Chem C. 2007; 111:175.
18. Sengupta B, Ritchie CM, Buckman JG, Johnsen KR, Goodwin PM, Petty JT. J Phys Chem C. 2008; 112:18776.
19. Soto-Verdugo V, Metiu H, Gwinn E. J Chem Phys. 2010; 132:195102. [PubMed: 20499990]
20. Richards CI, Choi S, Hsiang JC, Antoku Y, Vosch T, Bongiorno A, Tzeng YL, Dickson RM. J Am Chem Soc. 2008; 130:5038. [PubMed: 18345630]
21. Sharma J, Yeh HC, Yoo H, Werner JH, Martinez JS. Chem Commun. 2010; 46:3280.
22. Petty JT, Fan C, Story SP, Sengupta B, StJohn Iyer A, Prudowsky Z, Dickson RM. J Phys Chem Lett. 2010; 1:2524. [PubMed: 21116486]
23. O'Neill PR, Velazquez LR, Dunn DG, Gwinn EG, Fygenson DK. J Phys Chem C. 2009; 113:4229.
24. Sengupta B, Springer K, Buckman JG, Story SP, Abe OH, Hasan ZW, Prudowsky ZD, Rudisill SE, Degtyareva NN, Petty JT. J Phys Chem C. 2009; 113:19518.
25. Lavis LD, Raines RT. ACS Chem Biol. 2008; 3:142. [PubMed: 18355003]
26. Bloomfield, VA.; Crothers, DM.; Tinoco, J.; Ignacio. Nucleic Acids: Structures, Properties, and Functions. University Science Books; Sausaltio, CA: 2000.
27. Texier I, Goutayer M, Da Silva A, Guyon L, Djaker N, Josserand V, Neumann E, Bibette J, Vinet F. J Biomed Opt. 2009; 14:054005. [PubMed: 19895107]
28. Philip R, Penzkofer A, Bäumler W, Szeimies RM, Abels C. J Photochem Photobiol, A. 1996; 96:137.
29. Vosch T, Antoku Y, Hsiang JC, Richards CI, Gonzalez JI, Dickson RM. Proc Natl Acad Sci U S A. 2007; 104:12616. [PubMed: 17519337]
30. Rigler R, Mets U, Widengren J, Kask P. Eur Biophys J Biophys Lett. 1993; 22:169.
31. Carmichael I, Hug GL. J Phys Chem Ref Data. 1986; 15:1.
32. Yip WT, Hu D, Yu J, Vanden Bout DA, Barbara PF. J Phys Chem A. 1998; 102:7564.
33. Krichevsky O, Bonnet G. Rep Prog Phys. 2002; 65:251.
34. Widengren J, Seidel CAM. Phys Chem Chem Phys. 2000; 2:3435.
35. Henglein A, Mulvaney P, Linnert T. Faraday Discuss. 1991:31.

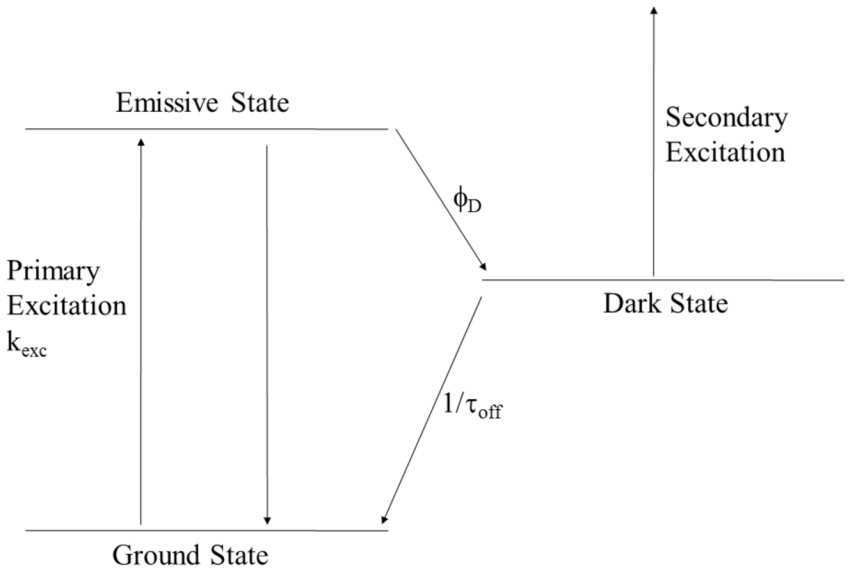

Figure 1.

Schematic energy level diagram rationalizing the photophysical behavior of the cluster-DNA conjugates. Fluorescence is derived from cycling through the ground and emissive states using both primary and secondary laser excitation. Inverse transition rates into and out of the dark state define τ_{on} and τ_{off}, respectively. Decay from the dark state occurs by both natural decay and optical excitation. The entrance time into the dark state τ_{on} is the inverse of the product of the dark state quantum yield (φ_D) with the excitation rate (k_{exc}).

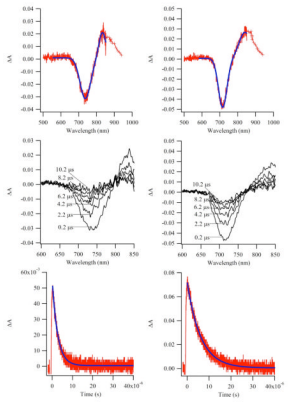

Figure 2.

Time-resolved transient absorption spectra and kinetic decays for the 800 nm emitting silver clusters that form with $C_3AC_3AC_3\underline{T}C_3A$ (left) and $C_3AC_3AC_3\underline{G}C_3A$ (right). (Top) Spectra acquired in 2 μs increments after the laser pulse (740 nm, 700 μJ). The blue line is the fit of the ground state bleach and the excited state absorption bands. Discretely constructed spectra at longer wavelengths are indicated by the crosses and support the assignment of the λ_{max} for the excited state absorption. (Middle) Time evolution of the spectra with isosbestic points at 801 nm (left, $C_3AC_3AC_3\underline{T}C_3A$) and at 778 nm (right, $C_3AC_3AC_3\underline{G}C_3A$). (Bottom) Kinetic traces show the decay of the excited state populations by monitoring the absorbance at 860 nm (left, $C_3AC_3AC_3\underline{T}C_3A$) and 850 nm (right, $C_3AC_3AC_3\underline{G}C_3A$). The time constants are 2.6 μs and 6.0 μs, respectively. These time constants do not depend on the absorbance wavelength being monitored.

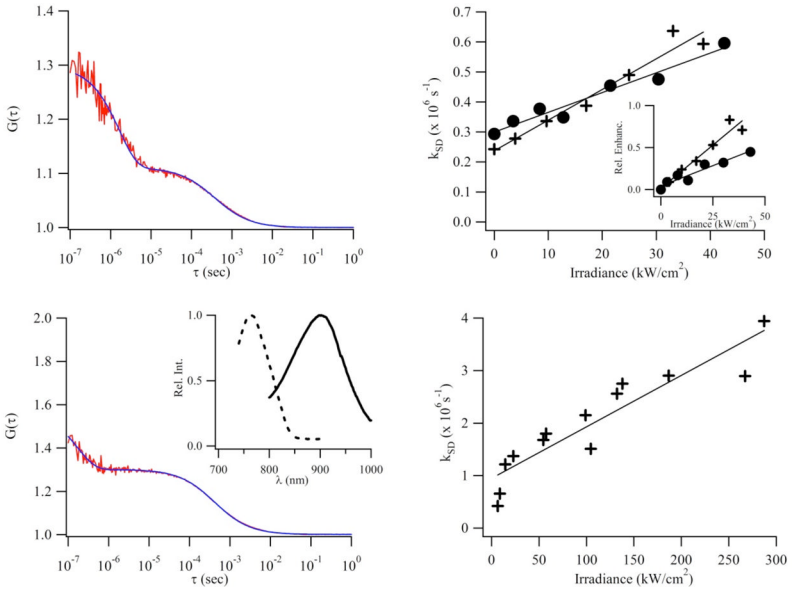

Figure 3.

(Top, left) Correlation function for the cluster associated with $C_3AC_3AC_3\underline{G}C_3A$ collected at an irradiance of 30 kW/cm_2 at 690 nm. (Top, right) The effect of irradiance at 905 nm (with a fixed irradiance of 30kW/cm^2 at 690 nm) on the dark state relaxation times for the clusters associated with $C_3AC_3AC_3\underline{G}C_3A$ (crosses) and $C_3AC_3AC_3\underline{T}C_3A$ (circles). The inset shows the dependence of the relative enhancement using primary excitation at 690 nm at 30 kW/cm^2 and varying irradiances at 905 nm for the $C_3AC_3AC_3\underline{G}C_3A$ (crosses) and $C_3AC_3AC_3\underline{T}C_3A$ (circles) – based clusters. (Bottom, left) Correlation function for the cluster associated with $C_3AC_3AC_3AC_3\underline{G}$ collected at an irradiance of 60 kW/cm^2 at 840 nm. The inset contrasts the spectra for the distinct clusters associated with $C_3AC_3AC_3\underline{G}C_3A$ (dashed line) using λ_{ex} = 720 nm and $C_3AC_3AC_3AC_3\underline{G}$ (solid line) using λ_{ex} = 840 nm. (Bottom, right) The 840 nm irradiance dependence of the dark state relaxation times for the clusters associated with $C_3AC_3AC_3AC_3\underline{G}$.

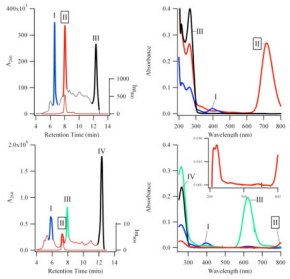

Figure 4.

(Top left) Chromatograms derived using the absorbance at 260 nm (left axis) and fluorescence intensity (cps) using λ_{ex} = 720 nm and λ_{em} = 800 nm (right axis) for the cluster-$C_3AC_3AC_3\underline{G}C_3A$ conjugates. The near infrared emissive species is associated with Peak II. (Top right) Spectra associated with peaks in the chromatogram on the left. (Bottom left) Chromatograms derived using the absorbance at 260 nm (left axis) and fluorescence intensity (cps) using λ_{ex} = 840 nm and λ_{em} = 870 nm (right axis) for the cluster-$C_3AC_3AC_3AC_3\underline{G}$ conjugates. The near infrared-emissive species is associated with Peak II. (Bottom right) Absorption spectra associated with peaks in the chromatogram on the left. The inset expands the view for the spectrum of the near infrared emitter. Note that the spectral capabilities of the instrument absorption do not extend beyond 800 nm.

Table 1

Comparison of measured τ_{on} and τ_{off} for the dark state associated with the near-infrared emitting clusters that form with $C_3AC_3AC_3\underline{T}C_3A$ and $C_3AC_3AC_3\underline{G}C_3A$. Primary excitation at 690 nm has fixed irradiance (30 kW/cm^2)[a] and secondary excitation is at 905 nm with varying irradiance.

$C_3AC_3AC_3TC_3A$			$C_3AC_3AC_3GC_3A$		
Secondary laser irradiance (kW/cm^2)[a]	**τ_{on} (μs)**	**τ_{off} (μs)**	**Secondary laser irradiance (kW/cm^2) [a]**	**τ_{on} (μs)**	**τ_{off} (μs)**
0	2.7	3.4	0	1.9	4.1
3	2.0	3.0	4	1.9	3.6
8	1.8	2.7	10	1.9	3.0
13	1.8	2.9	17	1.9	2.6
21	1.8	2.2	25	1.9	2.0
30	1.9	2.1	33	1.5	1.6
43	2.1	1.7	39	1.8	1.7

[a]Irradiance values derived from the average intensity in the FCS focal volume.

Table 2

Comparison of measured τ_{on} and τ_{off} for the dark state associated with the near-infrared emitting clusters that form with $C_3AC_3AC_3AC_3\underline{G}$. Primary excitation at 840 nm is varied with no secondary illumination.

Primary laser irradiance (kW/cm^2)	τ_{on} (μs)	τ_{off} (μs)
6	17.5	2.4
9	8.7	1.5
14	2.3	0.8
23	1.6	0.8
55	0.9	0.6
57	1.0	0.6
102	0.8	0.5
132	0.7	0.4
138	0.4	0.4
187	0.5	0.3
267	0.4	0.3
287	0.5	0.3